C-amidation of substituted β³ oligoamides yields novel supramolecular assembly motif

Claire Buchanan[a], Ljiljana Puskar[b], Christopher J Garvey[c,d], and Adam Mechler*[a]

[a.] *Department of Chemistry and Physics, Latrobe University, Bundoora, Australia.*
[b.] *Helmholtz Zentrum Berlin für Materialien und Energie GmbH, Berlin, Germany.*
[c.] *Forschungs-Neutronenquelle, Heinz Maier-Leibnitz Zentrum (FRM II), Technische Universität München, Lichtenbergstraße 1, 85748 Garching, Germany.*
[d.] *Lund Institute for Advanced Neutron and X-ray Science, 223 70 Lund, Sweden*

Electronic Supplementary Information (ESI) available: [Infrared spectroscopy of Ac-β³[LIA], β³[LIA]-$CONH_2$ and β³[LIA] in the 2800 nm to 3800 nm region]. See DOI: 10.1039/x0xx00000x

Abstract

N-acylated substituted β³ oligoamides are known to form unique supramolecular nanorods based on a 3-point hydrogen bond self-assembly motif. This motif is an intermolecular extension of the hydrogen bonding network that stabilizes the 14-helix secondary structure unique to β³ oligoamides. Acetylation of the N-terminus of the molecule provides the necessary third hydrogen bond pair of the motif. Here, the possibility of introducing the third hydrogen bond pair *via* amidation of the C terminus is investigated. While similar in purpose, this modification introduces a chemically distinct new self-assembly motif, also removing the bulky carboxyl group that does not fold into the 14 helix positioning instead as a side chain. Three substituted β³ oligoamide variants with the base sequence LIA (where the letters denote β³ residues with side chains analogous to α amino acids) were compared: N-acylated Ac-β³[LIA] as a reference, C-amidated β³[LIA]- $CONH_2$, and β³[LIA] with free unmodified N and C termini as a negative control. The three variants were dissolved in water to promote self-assembly. The self-assembly was characterised using mid- and far-infrared spectroscopy, small angle x-ray scattering (SAXS) and atomic force microscopy (AFM). IR measurements confirmed that all three samples were in a similar conformation, consistent with pseudo 14-helical secondary structures. Far-infrared spectroscopy measurements of β³[LIA]- $CONH_2$ showed distinct peaks consistent with highly organised skeletal modes, i.e., regular supramolecular assembly, that was largely absent from the other two oligoamides. Modelling of SAXS data is consistent with elliptical cylinder structures resulting from nanorod bundling for both β³[LIA]- $CONH_2$ and Ac-β³[LIA], but not in the unmodified sample. Consistently, AFM imaging showed large nanorod bundling structure in β³[LIA]- $CONH_2$, varied bundling structures in Ac-β³[LIA], and only aggregation in β³[LIA]. Amidation showed much more organised and robust assembly compared to acetylation, providing a new, easy to synthesize self-assembly motif for helical nanorod assembly that is similar but distinct to N-acylation

Introduction

Bottom-up nanofabrication is a collective name for the formation of complex, pre-defined structures from discrete subunits following self-assembly principles, for efficient, replicable generation of nanostructured materials.[1-3] The predefined superstructure geometries are encoded by the physico-chemical properties of the structural subunits and the conditions under which the assembly occurs.[1-3] For self-assembly to be truly effective, careful design of appropriate subunits is key.[1-3] Substituted oligoamides (synthetic analogues to natural peptides) based on β³ amino acids were shown to be suitable subunits to form nano-to-micrometer scale fibrous self-assembled structures.[4-9] β³ amino acids hold strong similarities to natural amino acids, with the characteristic difference of an additional methylene group in the carbon backbone of the molecule; as such, the side chains of these amino acids can be described using standard α amino acid nomenclature.[10-12] β³ oligoamides (also known as β³-peptides) fold spontaneously into several different types of helical secondary structures.[11-14] Of these, the 14-helix (that contains 14 atoms in one loop from H-bond donor to acceptor) is the most interesting for self-assembly due to its superior stability and unique properties.[15-20] The 14-helix is formed and stabilised through hydrogen-bonding of amides between residues *i – i+3*, and has a pitch of 3-3.1 residues per turn, resulting in the alignment of every 4th residue to form three "faces" of the structure. Studies have shown that the 14-helix structure is stable with as little as four residues, i.e. with a single intramolecular hydrogen bond.[21-24]

The acylation of the N-terminus of the oligoamides leads to the head-to-tail assembly of the helices into long fibrils, also described as nanorods, through an intermolecular H-bonding pattern that mimics the 14-helix core motif, where the amide formed with the acyl group provides the necessary third hydrogen bond donor.[10, 23-25] This motif is very strong and self-assembly occurs regardless of the chemistry of the sidechains present and/or residue sequence.[23-24, 26-27] The fibrils further assemble into an array of diverse structures ranging from a few nm to hundreds of nm in diameter. The properties of the distinct faces of the nanorods, determined by the primary structure of the oligoamide, strongly affect the assembly of the helices into these superstructures through van der Waals interactions and solvophobic effects.[9, 23-24, 28-29] Remarkably, the motif is also maintained in oligoamides as short as three amino acids, which are unable to form a full helical loop due to their insufficient length.[21-24] Previous X-ray crystallography and Far IR spectroscopy studies suggested that these tri-oligoamides form curved "horseshoe" shaped structures that assemble head-to-tail to form a '14-helical-like' structure with comparable steric strain to its 14-helical counterparts (figure 1).[22, 25] The oligoamide Ac-β³[LIA] in particular has shown to consistently form large scale supramolecular structures

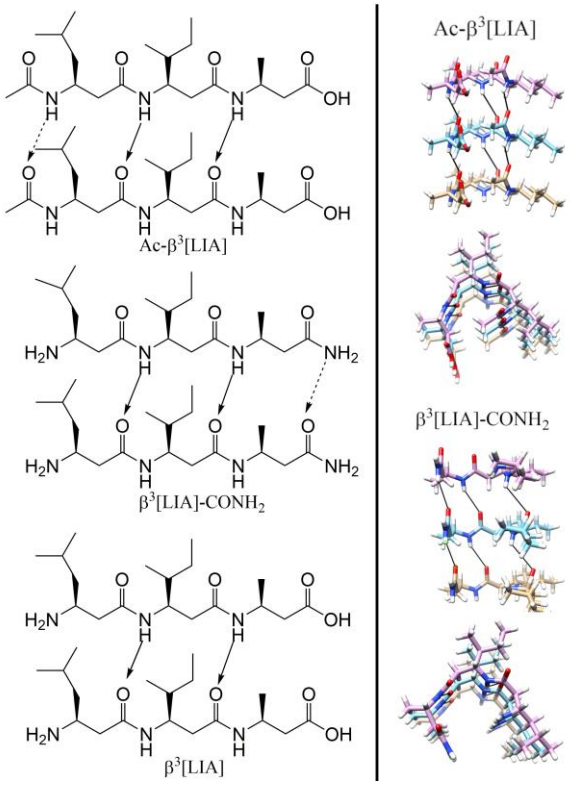

Figure 1. Structure of three substituted oligoamides based on the β³-amino acid sequence LIA, along with proposed 3-point bonding motif. Dash arrow indicates H-bond created by terminal modifications. Right hand side shows 3D models of expected 14-helcal loop folding and stacking to form fibrils from Ac- β³[LIA] and β³[LIA]-CONH₂

exhibiting various geometries highly dependent on solvent properties.[21-24] Far IR and computational studies on "scrambled" tri-oligoamides differing only in amino acid sequence show no change in the sterics of the horseshoe conformation.[22] These helical-like structures consist of 4 faces as opposed to the three normally seen in 14 helices; in addition to the three faces created through residues alignment, the terminal carboxyl group forms the fourth face in the fibres as it cannot sterically fit in the pseudo-helical loop, and hence bends outward due to the high conformational flexibility of the beta amino acid backbone.[22, 25] The strength and versatility of this supramolecular H-bonding motif can be attributed to the third H-bond pairing provided by the addition of the third H-bond donor amide group formed via acylation.[10, 25] Based on the confirmed success of this principle, there is a potential second method of creating the third H-bonding pair by the amidation of the C-terminus of the oligoamide.[10, 21-27] This would form an amide moiety at the C terminal end of the molecule, in a way common to natural peptides. C-terminal amidation is a simpler synthetic process compared to N-terminal acylation. In this work, N-terminal acylation and C-terminal amidation are compared on the basis of the well characterized tri-oligoamide β³[LIA] (Figure 1), in order to determine if assembly can occur via the proposed motif, and if the proposed and the established motifs exhibit the same self-assembly behaviours. Morphological analysis is performed using atomic force microscopy and small angle X-ray scattering to determine the supramolecular shapes formed in solid and solution phase, respectively, while both far- and mid-infrared spectroscopy is used to glean further insights of the secondary structures present.

Experimental

Materials

Three substituted oligoamides were characterised in this study. The three oligoamides share the same base structure, denoted by standard peptide nomenclature as β³Lβ³Iβ³A (leucine, isoleucine, alanine) or β³[LIA] for short, and differ in their termini. Ac-β³[LIA] sample has N-terminus acetylation, β³[LIA]-$CONH_2$ has C-terminus amidation, while the unmodified oligoamide β³[LIA] has no modifications of either termini (Figure 1). Ac-β³[LIA] has been well characterised previously [21-24, 27, 30-31] and is included here as a direct reference. β³[LIA]-$CONH_2$ contains the proposed new self-assembly motif. β³[LIA] is used as a negative control to confirm that nanorod formation cannot occur without the third amide moiety.

Substituted oligoamides were synthesised using standard solid phase synthesis as previously described from L-β³-amino acids.[25] The C-amidation was achieved by conducting synthesis on Rink amide resin, while the unmodified and N-acetylated samples were synthesised on Wang resin. Acetylation was performed post synthesis, but before resin cleavage as previously described.[25]

Methods

Far-Infrared Spectroscopy. All far-IR measurements were conducted at the Australian synchrotron, using the ATR set-up on the Far IR beamline. Samples of concentrated oligoamides in water were deposited in 0.5 µl increments and dried with nitrogen gas on a diamond ATR disc until the amount of material was sufficient to be detected. Measurements were conducted in the 50-600 cm^{-1} spectral region. Spectra were recorded using the synchrotron light source with an IFS 125/HR Bruker spectrometer coupled to a Si Bolometer cooled with liquid He. The beam aperture was set to 12.5 µm and 200 scans were recorded per spectra with a resolution of 1 cm^{-1}. Backgrounds were recorded on the clean ATR disc before sample deposition using the same settings and collecting 400 scans. Analysis was performed by averaging 7-10 spectra for each sample using OPUS software (Bruker). Final plots were produced in Origin (Pro) Version 2018 (OriginLab Corporation, Northampton, MA, USA)

Mid-Infrared Spectroscopy. All mid-IR measurements were performed at HZB using the BESSY II synchrotron IRIS beamline. Samples were deposited on ZnSe disc from isopropanol and allowed to dry at room temperature.

Data was collected on a N_2 gas purged Nicolet Continuµm Infrared Microscope (Thermo Scientific) coupled to a Nexus 870 FT-IR spectrometer using Cassegrain infrared reflective objectives. The experimental setup was coupled with a Linkam stage cell purged with nitrogen gas, and was cooled to -35 C° using liquid nitrogen. A knife edge aperture was used to set

synchrotron light source illumination to a 15 x 15 µm area. 128 scans were collected at each sample measurement point, with a 4 cm^{-1} resolution using OMNIC Atlµs™ software. Background measurements were collected through a nearby clean area of the ZnSe using 256 scans. The spectra with the most intensity was used for each sample, and final plots were prepared using Origin(Pro) software.

Atomic Force Microscopy. Two sample solutions of each oligoamide were prepared by dissolving in either water or isopropanol to 1mg/ml concentration. Samples were incubated at 37°C for 1 week before deposition on freshly cleaved mica. Each solution was deposited and dried under two conditions. A "slow drying" method was achieved by depositing the sample and drying at 37°C overnight, while an "instant dry" method was achieved by purging sample for 15 minutes with argon gas directly after deposition, followed by immediate AFM imaging.

All AFM imaging was conducted using the Ntegra AFM platform and software (NT-MDT, Zelenograd, Russia). Semi-contact mode was used for all imaging, using silicon probes with 140-390 kHz resonance frequencies (force constant of 3-37 N/nm). All data processing was performed with Gwyddion software (www.gwyddion.net, Czech Metrology Institute).

Small Angle X-ray Scattering (SAXS). SAXS spectra of the three samples were collected on the SAXS/WAXS beamline[32] at the Australian Synchrotron in a beamline configuration especially for collecting background subtracted absolutely scaled scattered intensity, I(q). Samples were dissolved in water to a concentration of 1 mg/ml and left to mature for at least 12 months at 4° C. β^3 oligoamides are chemically stable and hence the prolonged storage/aging does not cause any noticeable degradation. The solutions were aspirated into 1mm quartz crystal capillaries, and 10 x 1 s measurements were taken at 7 m distances between Pilatus 1M detector (Dectric, Baden, Switzerland) and the sample. The isotropic 2-dimensional scattering patterns were background subtracted (capillary with water) and azimuthally averaged to the intensity versus scattering vector form, I(q) and normalised to absolute scale with a water sample for background using beamline software Scatterbrain.[33] The scattering vector defined $q = 2\pi/\lambda \sin(\theta)$ where λ is the wavelength of the X-rays (1.078 Å) and $\theta/2$ is scattering angle.

Structural information was extracted from the scattering curves by non-linear least squares model fitting with appropriate constraints was applied to data from all three samples using SASview (http://www.sasview.org/).[34] While the AFM data gives local insight into the types of shapes present in the samples on a surface, which can inform SAXS analysis, the analysis of SAXS gives a low resolution representation of the average structure in solution with little sample preparation. The aim of modelling is to give spatially averaged values for size, shape and particles present in the solution. The Ac-β^3[LIA] and β^3[LIA]-$CONH_2$ were fitted to an elliptical cylinder model[35-36], describing a flattened cylinder with a length factor, and a major and minor radius (supplementary information). The data generated from β^3[LIA] was modelled with a composite of two models to account for the extended scattering in the high Q region (cylinder model[36-37]), while the Low Q region was fitted with an ellipsoid model (supplementary information).

All model fitting was performed with the assumption that scattering was in the dilute limit, i.e. the form factor scattering (that is, scattering due to morphological envelopes of the suspended species). An important step in the modelling was to constrain the parameter space with physically reasonable values. Scattering length density values were calculated using IGOR software with the IrenaSAS macros[38]. Partial molar values for these calculations were found by using CRYSOL[39] and an appropriate PDB file. PDB files were obtained by modifying the side chains and terminal groups of a PDB crystal structure previously obtained of a tri-substituted oligoamide[25].

Results and Discussion

Infrared Spectroscopy

Far-Infrared Spectroscopy. Far-infrared amide bands appearing at 597-601 cm^{-1} and 466-470 cm^{-1} spectral ranges can be seen in all three samples (figure 2), and are most likely a combination of amide IV, V and VI bands due to C=O out-of-plane bending.[22-23, 40-41] These bands are highly sensitive to any tension in the structure and therefore the secondary structure, and hence the similarity of the peak positions in all three oligoamides indicates a highly consistent secondary structure, while the band positions match previously recorded spectra of three unit long substituted oligoamides.[22-23] A broad band can be seen at 100-300 cm^{-1} in both Ac-β^3[LIA] and β^3[LIA] that is not present in β^3[LIA]-$CONH_2$. This region corresponds to multiple vibrations that can potentially include CN rotational modes (amide VII) and skeletal modes.[22, 40-41] This band is at a position where water vibrations may also occur, however water as a source is highly unlikely: all samples were prepared under the same conditions, and if the band was caused by residual water it should be present in all three samples. Furthermore, the same basic preparation method for MIR data shows no water bands in the 3400 cm^{-1} (Supplementary information). All samples show very small but consistent peaks in this region, although the broad band obscures these peaks somewhat in the Ac-β^3[LIA] and β^3[LIA] samples. The presence of small but well defined peaks in this region for β^3[LIA]-$CONH_2$ indicates highly consistent structures, where these vibrational modes take place in a highly conserved chemical environment, i.e. regular structure. The broadening of these peaks in Ac-β^3[LIA] and into one broad band in β^3[LIA] indicates substantial variation in the local chemical environment, suggesting increasingly higher conformational flexibility. Thus, based on far-IR data, β^3[LIA]-$CONH_2$ has the most regular structure, indicating potentially crystalline, regularly packed material.

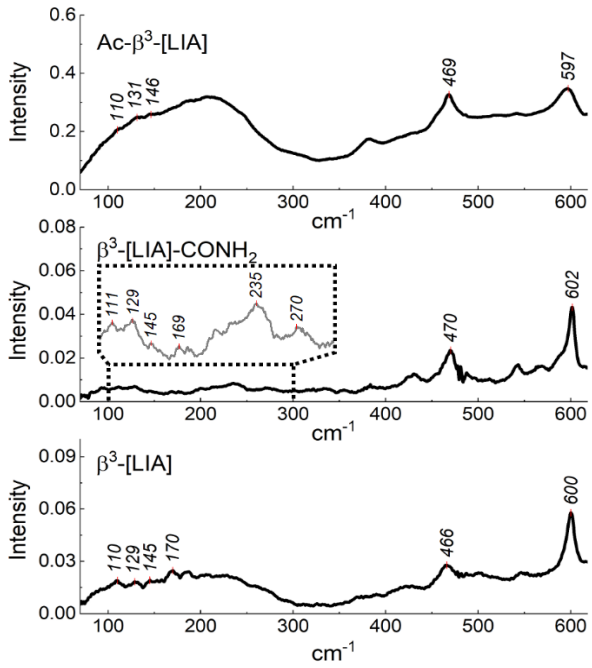

Figure 2. Far-infrared spectra of the three substituted oligoamide samples.

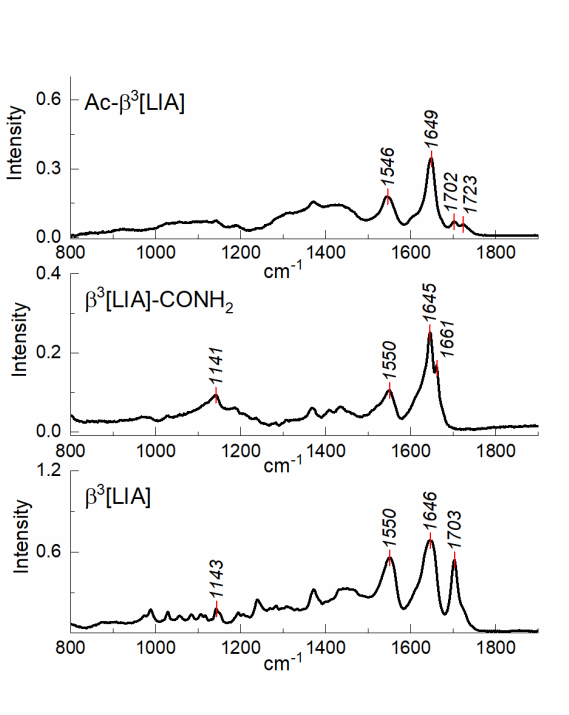

Fig. 3 Mid-infrared spectra of the three substituted oligoamide samples.

Mid-infrared Spectroscopy. The amide I and II bands can be seen at 1645-1649 cm^{-1} and 1545-1551 cm^{-1}, respectively, and are consistent across all three samples (figure 3). Amide I bands are mainly due to C=O stretch, while amide II bands are CN stretch and NH bending vibrations, and as such both are highly sensitive to the secondary structure of the oligoamides and are commonly used to determine secondary structures present in peptides.[42-47] As in case of the far-IR data the consistency in amide I and II band positions for all three samples indicates highly similar secondary structures, while the band positions match values previously associated with 14-helix confirmation, indicating that the secondary structure of the oligoamides is not affected by the terminal groups and does not require any intramolecular H-bonds to be in a 14-helix-like conformation, likely due to the steric effect of the bulk of the side chains.[26, 48-49] An absence of peaks at 3450 cm^{-1} and 3615 cm^{-1} (supplementary information) indicates no water molecules associated with the samples, and hence no interference with the amide I band.

The band at 1702-1724 cm^{-1} in Ac-β³[LIA] and β³[LIA] correspond to the C-terminal carboxyl group, and as expected it is not present in β³[LIA]-$CONH_2$.[26, 42-45, 47] The band at 1660 cm^{-1} in β³[LIA]-$CONH_2$ corresponds to N-H stretch vibration of the primary amine of the N-terminus.[42-45, 47] In the control sample this peak likely overlaps with the amide I peak, revealing more conformational flexibility. The CN stretch vibrations of the primary amide can also be seen at 1143-1142 cm^{-1}. This peak is absent in Ac β³[LIA], as expected. The remaining peaks in the 1000-1500 cm^{-1} region correspond to C-H vibrations of the side chain moieties and are consistent between each sample, as expected due to their identical sidechain moieties. Slight variations in this region suggest different intermolecular sidechain-sidechain interactions upon bundling, as seen in the far-IR region as well.

AFM

AFM imaging provides information of the morphological structures formed by the substituted oligoamides when dried. All samples were deposited atop of atomically smooth mica surface and thus the lowest (darkest) areas in the background show the exposed mica, and used as a reference to measure layer thicknesses. The images thus show that the material is spread in a very thin layer over the surface, with the exception of a few large fibrous aggregates.

Deposits were made from either water or isopropanol solvent under two conditions: slow dried, where the solvent was left to evaporate overnight under standard conditions, or “instant” dried, where the sample was immediately dried using a stream of argon gas for 15 minutes. In the slow dry method, (commonly used for AFM sample preparation) the natural evaporation of solvent gives a slowly increasing sample concentration, that could allow the increasingly concentrated sample to assemble. The “instant” dried method is used to prevent this evaporation dependant assembly, to show the structures as they exist in solution. The distinct differences between the slow and instant dried data sets indicates that a high level of assembly does occur during the standard AFM drying process, and hence the structures present here are expected to be distinct to those found in solution *via* SAXS. Water and isopropanol solvents were both used to test the robustness of hierarchical assembled structures under differing dielectric constants and solvophobic conditions, as previous work shows Ac-β³[LIA] to be highly sensitive to these factors.[21, 23-24]

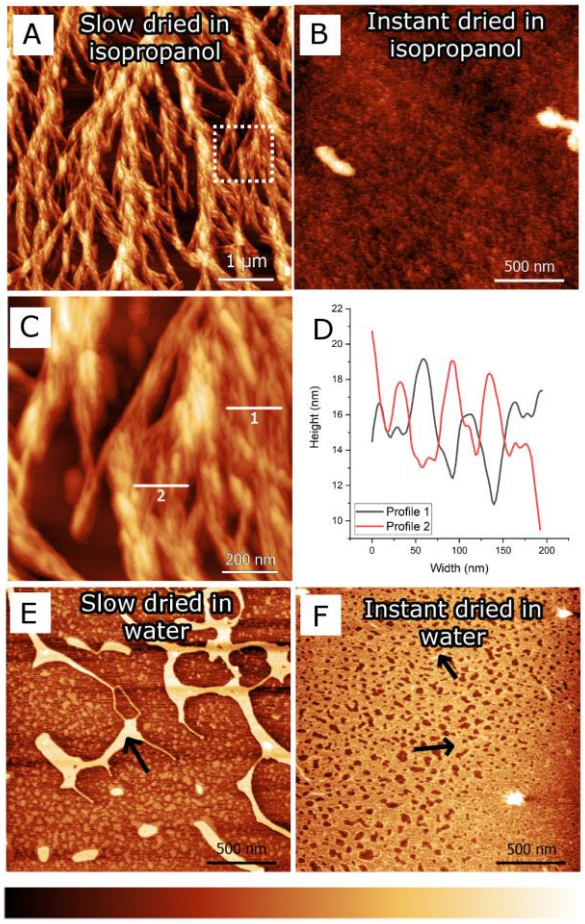

Figure 4. AFM images of Ac-β3[LIA]. A & B depict sample deposited from isopropanol. Images E & F depict sample deposited from water. A & E were prepared using the slow dry method, while B and F were prepared using the instant dry method. C depicts higher resolution scan of area depicted in A by dotted lines, and D shows the hight profiles of the lines depicted in C. Arrows in E and F indicate areas of fibrous material where individual fibres are too tightly paced to be resolved. Colour scale gives structural height; (A) 40 nm, (B) 3.9 nm, (E) 5.5 nm, and (F) 2.4 nm. Darkest colour is the mica substrate surface.

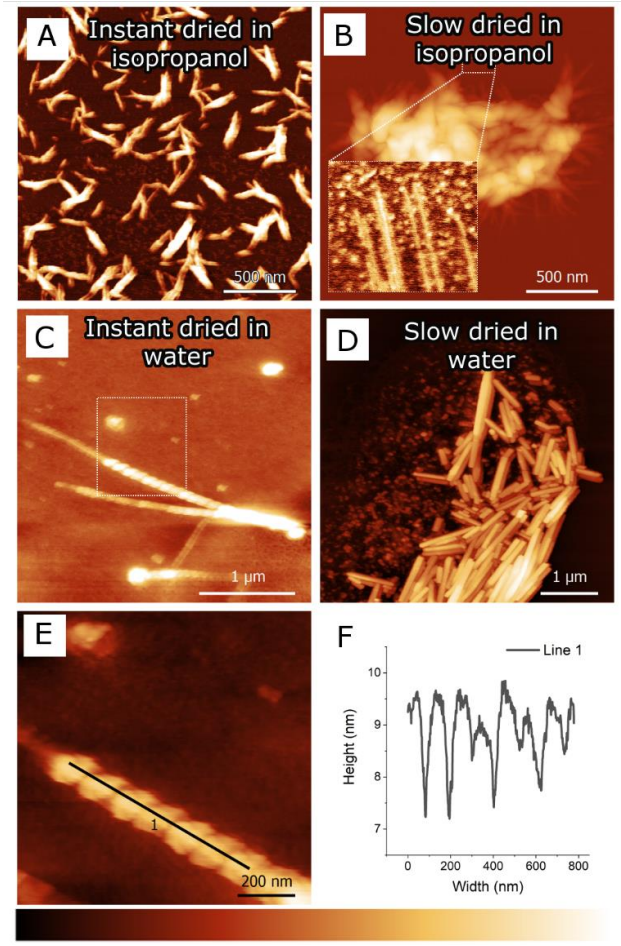

Figure 5. AFM images of the β^3[LIA]-$CONH_2$. A & B depict sample deposited from isopropanol. C - F depict sample deposited from water. A & C were prepared using the instant dry method, while B and D were prepared using the slow dry method. E depicts higher resolution scan of area shown in C by dotted lines, and F shows the height profiles of the lines depicted in E. Colour scale gives structural height; (A) 12.5 nm, (B) 300 nm, (C) 9.6 nm, and (D) 171 nm. Darkest colour in all cases is the mica substrate surface.

Ac-β³[LIA]. Ac-β^3[LIA] is shown for reference and also to benchmark the instant drying method. AFM images show large dendritic structures when slow dried from isopropanol (figure 4A), as previously reported.[21-24, 30-31] The low dielectric constant of isopropanol allows Van der Waals interaction to dominate, allowing the formation of these structures. A closer look at these structures reveals them to be entirely comprised of smaller, densely packed thin fibres (figure 4C & D). These fibres and dendritic structures are not seen when the sample is instantly dried (figure 4 B): the deposit appears to show a smooth layer, implying that the dendritic structures appear when the solution is concentrated during drying while the dilute nature of the bulk solution shifts the self-assembly equilibrium towards the individual fibres and small oligomers. It was shown before that larger fibres do form in the solution phase, however based on these AFM images fibrous form might not be the dominant structure. When deposited from water, solvophobic interactions dominate the assembly. Instant drying yields an organised oligoamide layer of around 1 nm thickness, with small visible fibres of 2 nm diameter and up to 0.1 µm length (figure 4 F). When allowed to slow dry, a somewhat random system of larger structures of up to 6 nm height can be seen from which small fibres (1 uM length) protrude, indicating that these are islands formed from bundles of the smaller fibres as described before (Figure 4 E)..[21-24, 30-31]

β³[LIA]-$CONH_2$. The C-amidated oligoamide shows increased fibrous assembly in both solvents and under both fast and slow drying conditions (figure 5), albeit with lesser dendritic and larger assembly structures. This indicates that solvent and drying (and hence concentration) effects have less effect on assembly, possibly due to more formed structures in solution that are less susceptible to change by environmental factors
When instant dried from isopropanol (figure 5A), β^3[LIA]-$CONH_2$ forms a layer of short fibres of 20 nm diameter and 0.25µm length, which clump together upon slow drying to form bundles of ~12 nm height (figure 5B). Instant drying from

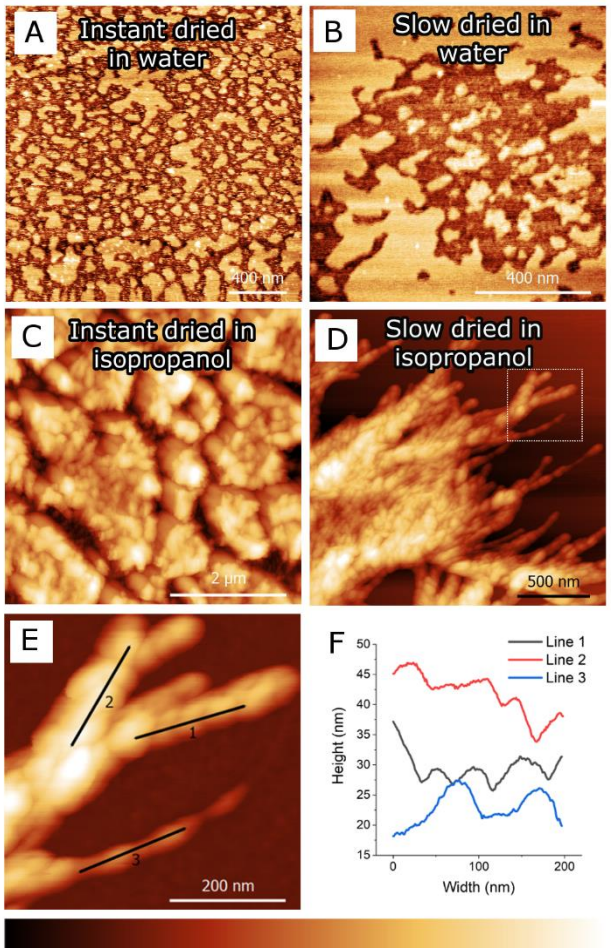

Figure 6. AFM images of β³[LIA]. A & B depicts sample deposited from water. C & D depicts samples deposited from Isopropanol. A & C were instant dried, while B and D were slow dried. E depicts higher resolution scan of area depicted in D by dotted lines, and F shows the hight profiles of the lines depicted in E. Colour scale indicates height: (A) 1.5 nm, (B) 2.0 nm, (C) 96 nm, and (D) 77 nm. Darkest colour is the mica substrate surface.

water (figure 5 C) is mostly amorphous but the deposit also contains a few long hierarchical fibre bundles of 2-10 µm length and around 20 nm thickness that offers a clear view of the hierarchical self-assembling nature of the sample in the solvent phase. Close inspection of these fibres (figure 5 E & F) reveals regular, periodic grooves every 50 nm and indicates a highly structured winding of fibres to form larger structures. Thus C-amidation promotes nanorod formation better than N-acylation for this oligoamide sequence. The slow dried samples show areas of high concentration of short fibres, forming aggregations of up to 300 nm height (figure 5 B & D).

β³[LIA]. As expected, most sample preparation methods show nonspecific aggregation of β³[LIA] (figure 6 A-C), consistent with the notion that the third amide moiety is essential for nanorod formation. However, when slow dried from isopropanol β³[LIA] unexpectedly developed large aggregates of dendritic appearance (figure 6 D) similar to those formed by Ac-β³[LIA] under the same conditions. However, these structures are noticeably different in that they do not show the defined small fibres found in the structures formed by Ac-β³[LIA]. A closer view instead reveals irregular, globular like definitions, which is consistent with an aggregation-based structure (Figure 6 E & F). The presence of such dendritic structures suggests that the overall geometry is the product of the drying process in the presence of isopropanol, likely driven by Van der Waals interactions of amorphous aggregates of the oligoamide in the gradually increasing concentration. It is notable that the same overall geometry appears much more fibrous in the Ac-β³[LIA] case while remains amorphous in β³[LIA], suggesting that the local high concentration of the oligoamides leads to the fibrous self-assembly in the former.

SAXS

SAXS data of the three oligoamides dissolved in water provides information of the morphological structures present when each oligoamide is in an aqueous environment and yields distinct morphological envelopes for each oligoamide sample. Observing the raw data (Figure 7) Ac-β³[LIA] and β³[LIA]-$CONH_2$ both showed high error margins in the high Q region where background scattering overpowered the isotropic scattering pattern, indicating the absence of a measurable population of species small enough to scatter in the higher Q regions. In contrast, β³[LIA] showed clear isotropic scattering in

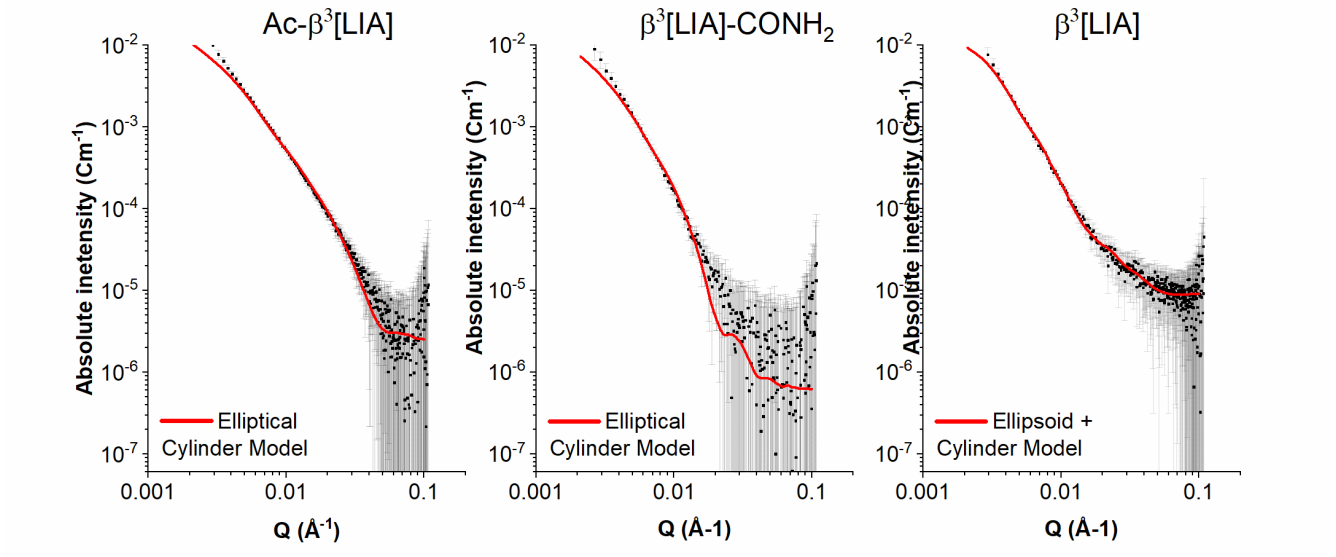

Figure 7. SAXS data and model fitting of all three samples using ellipsoid, triaxial ellipsoid and elliptical cylinder models for the acetylated and amidated sample, and the combined ellipsoid and cylindrical double model for the unmodified sample.

Table 1. Size and shape parameters from model fitting of SAXS data of Ac-β^3[LIA], β^3[LIA]-$CONH_2$, and β^3[LIA]

	Elliptical Cylinder Model			
	Minor Radius (nm)	*Major Radius (nm)*	*Length (nm)*	*% of Total Sample*
Ac-β^3[LIA]	*6.63 ± 0.14*	*48.1 ± 3.3*	*1,347.9 ± 153.2*	*4.69×10^{-2} ± 1.07×10^{-3}*
β^3[LIA]-$CONH_2$	*16.36 ± 0.48*	*59.8 ± 7.4*	*4,138.6 ± 429.8*	*9.18×10^{-3} ± 2.94×10^{-4}*
	Ellipsoid plus Cylinder Model			
	Ellipsoid Model (low Q)			
	Minor Radius (nm)	*Major Radius (nm)*	*% of Total Sample*	
β^3[LIA]	*22.89 ± 0.93*	*90.35 ± 7.58*	*9.39[3] ± 3.67×10^{-4}*	
	Cylinder Model (high Q)			
	Radius (nm)	*Length (nm)*	*% of Total Sample*	
	5.45 ± 0.62	*4354.7 ± 545.1*	*1.00×10^{-2} ± 1.99×10^{-3}*	

the high Q region, indicating the presence of a population of smaller oligomers. This follows the trend found from AFM imaging of instant dried water samples where β^3[LIA]-$CONH_2$ showed greatest degree of assembly, while as expected β^3[LIA] was largely amorphous. Thus, SAXS data is consistent with the importance of the three hydrogen bonding pairs for self-assembly.

Fitting the low Q region of the samples yielded slopes of -2.5 to -3, which is inconsistent with the expected slope of -1 for elongated anisotropic structures. However, this is most likely due to the highly variable length dimension, confirmed by AFM imaging, where both very long and very short fibrous structures are expected to coexist in accordance with the head-to-tail assembly motif. Model fitting is thus based on AFM evidence of the fibrous material to avoid mis-identifying the geometries due to polydispersity. Ac-β^3[LIA] and β^3[LIA]-$CONH_2$ samples yield a population of cylindrical structures (fibres) with well-defined and consistent radii, but with highly variable lengths. Thus, initially a simple cylinder model was applied, but was found impossible to fit. However, an elliptical cylinder model, which allows for flattened cylindrical structures, could be fitted to the scattering curves with good accuracy. Fitting of Ac-β^3[LIA] shows that 4.69 X 10^{-2} % ± 1.07 X 10^{-3} % of the sample assemble into elliptical cylinders with an average minor radius value of 6.63 nm ± 0.014 nm, a major radius value of 48.08 nm ± 3.32 nm, and a length value of 1,347.9 nm ± 153.15 nm. Fitting of β^3[LIA]-$CONH_2$ shows that 9.18 X 10^{-3} % ± 2.94 X 10^{-4} % of the sample forms somewhat larger elliptical cylinders with an average minor radius value of 16.36 nm ± 0.48 nm, a major radius value of 59.75 nm ± 7.44 nm, and a length value of 4,138.6 nm ± 429.75 nm. This is a surprisingly small fraction for both samples; the remaining material forms structures the sizes of which fall outside of the Q range of the measurement, i.e. the oligoamides are either in monomeric/small oligomeric form or in very large fibre bundles (that have been observed before by optical microscopy), and hence not detected using this method. That is not a shortcoming, however, as the aim of the SAXS measurements was to compare the fibrous assemblies in solution at a size range comparable to AFM measurements.

Additionally, the length values are likely to have a larger distribution from the mean than this model accounts for, due to the head-to-tail assembly motif of the oligoamides. It can therefore be concluded from this data that while the length factor is far too variable to give any meaningful values, both Ac-β^3[LIA] and β^3[LIA]-$CONH_2$ samples exist in water as asymmetrical fibre bundles with cross section radii of approximately 6.63 nm by 48.08 nm, and 16.36 nm by 59.75 nm, respectively.

The data from β^3[LIA] could not be fitted accurately with any one of these models, possibly due to the isotropic scattering curve in the high Q region. Modelling was then attempted assuming two populations coexisting in the sample; a less assembled population that scatters in the high Q region, and a population of larger structure in the lower Q region.

Fitting was successful with a combined model consisting of ellipsoid and cylinder models (eq. II). The ellipsoid model corresponds to the larger population, with radii values of 21 nm x 78 nm consistent with the random aggregation seen *via* AFM (figure 6), accounting for 1.15 X 10^{-2} % ± 3 X 10^{-4} % of the total sample mass. The cylinder model gives a radius value of 4 nm and length value of 6000 nm (Figure 7), accounting for 1.24 X 10^{-2} % ± 1.99 X 10^{-3} %. These values are unexpected as no similar structure is seen with AFM, indicating linear aggregation of β^3[LIA] into structures that do not survive the drying process, suggesting very weak interactions compared to the supramolecular self-assembly. These structures are consistent with micellar assemblies in water due to the polar backbone and non-polar side chains of the oligoamide. During sample preparation substantial foaming was noticed when mixing in water; this is consistent with surfactant behaviour and thus micellarization.

Discussion

β^3 substituted oligoamides are well documented to form 14-helix structures with a minimum of 4 backbone amides that is provided by 5 residues with free termini, or 4 if N-acylated, to complete a single loop of the helix.[11-12, 14, 50-52] Although N-acylated tri-β^3 oligoamides are lacking the 4th amide moiety to directly form 14-helices, previous work has shown that these oligoamides naturally arrange in a "horseshoe" conformation, which is similar in shape to a loop of the 14-helix found in larger oligoamides.[22-23] The fold can be confirmed indirectly from IR measurements: the peak positions of the amide IV-VI bands in the far IR and amide I and II bands in the mid-IR are specific to 14-helix/like confirmation, that was consistently identified in all three molecules in this study, strongly

suggesting that all samples are in this 14-helix-like confirmation.[22-23, 26, 48-49] The subsequent nanorod and consecutive bundling assembly however are dramatically different depending on the oligoamide end group.

The IR, AFM, and SAXS data combine to show a unique assembly preference for each sample. As expected, β^3[LIA] shows the least evidence of any regular assembly, with mostly mono/small oligomeric background with some random aggregation structures seen *via* AFM under dry condition (with the notable exception of the dendritic structures produced in the slow dried isopropanol sample), and no evidence of nanorod formation. The IR data shows broad bands in the 100-300 cm^{-1} region indicating no regular bundling structures, and the SAXS data also shows irregular assembly and some micellarization in solution. Hence, the lack of the third hydrogen bonding pair does limit the ability of the peptide to self-assemble into regular structures.

Ac-β^3[LIA], consistent with former observations[21-24, 30-31], shows clear signs of hierarchical assembly which can be seen *via* the winding visible on AFM images, and from SAXS data modelling which indicates the presence of fibrous structures in solution. It should be noted that, as also observed before, the variety of structures under dry conditions seen *via* AFM imaging, coupled with the broad band at 100-300 cm^{-1} in the far IR spectra indicates relatively high flexibility in the supramolecular interactions and therefore a high variability of the possible bundling/superstructures.

β^3[LIA]-$CONH_2$ forms the most consistent structures of all the samples. Although AFM imaging reveals some differences in each set of drying conditions, each show highly regular large bundles, with clear evidence of winding and hence hierarchical structures. The Far IR region of 100-300 cm^{-1} shows regular, well defined bands, indicating highly restricted chemical environments due to regular supramolecular structures. SAXS model fitting yields consistent, regular elliptical cylinder structures in solution. Hence, β^3[LIA]-$CONH_2$ shows a high level of regular structures at all levels of assembly, with both nanorods and regular bundles evident.

Conclusions

In conclusion, C-terminal amidation results in nanorod formation in substituted oligoamides that is comparable, and potentially superior to N-terminal acylation. Thus, C-terminal amidation offers an easier, quicker synthetic option to initiate nanorod formation and further hierarchical assembly of substituted oligoamides.

Author Contributions

All authors contributed to the conceptualisation, investigation, and review and editing of this work. Claire Buchanan wrote and visualised the original draft, and Adam Mechler supervised the project.

Conflicts of interest

There are no conflicts to declare.

Acknowledgements

We thank HZB for the allocation of synchrotron radiation beamtime. Measurements were carried out at the IRIS instrument on the BESSYII beamline at Helmholtz-Zentrum Berlin für Materialien und Energie.

We thank ANSTO for the allocation of beamtime. Part of this research was undertaken on the SAXS and THz - Far infrared beamlines at the Australian Synchrotron, part of ANSTO

This work benefited from the use of the SasView application, originally developed under NSF award DMR-0520547. SasView contains code developed with funding from the European Union's Horizon 2020 research and innovation programme under the SINE2020 project, grant agreement No 654000.

We acknowledge and thank Dr. Rania Seoudi for her prior work on these oligoamides; Figure 4 was based in part on her AFM data.

Notes and references

1. Narayanan, K. B.; Han, S. S., Helical plant viral nanoparticles-bioinspired synthesis of nanomaterials and nanostructures. *Bioinspir. Biomim.* **2017,** *12* (3), 20.

2. Liddle, J. A.; Gallatin, G. M., Nanomanufacturing: A Perspective. *ACS Nano* **2016,** *10* (3), 2995-3014.

3. Ariga, K.; Li, J. B.; Fei, J. B.; Ji, Q. M.; Hill, J. P., Nanoarchitectonics for Dynamic Functional Materials from Atomic-/Molecular-Level Manipulation to Macroscopic Action. *Adv. Mater.* **2016,** *28* (6), 1251-1286.

4. Wang, P. S. P.; Schepartz, A., beta-Peptide bundles: Design. Build. Analyze. Biosynthesize. *Chem. Commun.* **2016,** *52* (47), 7420-7432.

5. Wang, P. S. P.; Nguyen, J. B.; Schepartz, A., Design and High-Resolution Structure of a beta(3)-Peptide Bundle Catalyst. *J. Am. Chem. Soc.* **2014,** *136* (19), 6810-6813.

6. Martin, A. D.; Wojciechowski, J. P.; Robinson, A. B.; Heu, C.; Garvey, C. J.; Ratcliffe, J.; Waddington, L. J.; Gardiner, J.; Thordarson, P., Controlling self-assembly of diphenylalanine peptides at high pH using heterocyclic capping groups. *Scientific Reports* **2017,** *7*, 43947.

7. Del Borgo, M. P.; Kulkarni, K.; Aguilar, M. I., Using beta-Amino Acids and beta-Peptide Templates to Create Bioactive Ligands and Biomaterials. *Curr. Pharm. Design* **2017,** *23* (26), 3772-3785.

8. Luder, K.; Kulkarni, K.; Lee, H. W.; Widdop, R. E.; Del Borgo, M. P.; Aguilar, M. I., Decorated self-assembling beta(3)-tripeptide foldamers form cell adhesive scaffolds. *Chem. Commun.* **2016,** *52* (24), 4549-4552.

9. Wang, P. S.-P.; Craig, C. J.; Schepartz, A., Relationship between side-chain branching and stoichiometry in beta(3)-peptide bundles. *Tetrahedron* **2012,** *68* (23), 4342-4345.

10. Gopalan, R. D.; Del Borgo, M. P.; Mechler, A. I.; Perlmutter, P.; Aguilar, M. I., Geometrically Precise Building Blocks: the Self-Assembly of beta-Peptides. *Chem. Biol.* **2015,** *22* (11), 1417-1423.

11. Cheng, R. P.; Gellman, S. H.; DeGrado, W. F., beta-peptides: From structure to function. *Chem. Rev.* **2001,** *101* (10), 3219-3232.

12. Gellman, S. H., Foldamers: A manifesto. *Accounts Chem. Res.* **1998,** *31* (4), 173-180.

13. Appella, D. H.; Christianson, L. A.; Klein, D. A.; Powell, D. R.; Huang, X. L.; Barchi, J. J.; Gellman, S. H., Residue-based control of helix shape in beta-peptide oligomers. *Nature* **1997,** *387* (6631), 381-384.

14. Appella, D. H.; Christianson, L. A.; Karle, I. L.; Powell, D. R.; Gellman, S. H., beta-peptide foldamers: Robust Helix formation in a new family of beta-amino acid oligomers. *J. Am. Chem. Soc.* **1996,** *118* (51), 13071-13072.
15. Kritzer, J. A.; Tirado-Rives, J.; Hart, S. A.; Lear, J. D.; Jorgensen, W. L.; Schepartz, A., Relationship between side chain structure and 14-helix stability of beta(3)-peptides in water. *J. Am. Chem. Soc.* **2005,** *127* (1), 167-178.
16. Hart, S. A.; Bahadoor, A. B. F.; Matthews, E. E.; Qiu, X. Y. J.; Schepartz, A., Helix macrodipole control of beta(3)-peptide 14-helix stability in water. *J. Am. Chem. Soc.* **2003,** *125* (14), 4022-4023.
17. Raguse, T. L.; Porter, E. A.; Weisblum, B.; Gellman, S. H., Structure-activity studies of 14-helical antimicrobial beta-peptides: Probing the relationship between conformational stability and antimicrobial potency. *J. Am. Chem. Soc.* **2002,** *124* (43), 12774-12785.
18. Raguse, T. L.; Lai, J. R.; Gellman, S. H., Evidence that the beta-peptide 14-Helix is Stabilized by beta(3)-residues with side-chain branching adjacent to the beta-carbon atom. *Helv. Chim. Acta* **2002,** *85* (12), 4154-4164.
19. Raguse, T. L.; Lai, J. R.; LePlae, P. R.; Gellman, S. H., Toward beta-peptide tertiary structure: Self-association of an amphiphilic 14-helix in aqueous solution. *Org. Lett.* **2001,** *3* (24), 3963-3966.
20. Wu, Y. D.; Wang, D. P., Theoretical studies of beta-peptide models. *J. Am. Chem. Soc.* **1998,** *120* (51), 13485-13493.
21. Seoudi, R. S.; Hinds, M. G.; Wilson, D. J. D.; Adda, C. G.; Del Borgo, M.; Aguilar, M.-I.; Perlmutter, P.; Mechler, A., Self-assembled nanomaterials based on beta (beta(3)) tetrapeptides. *Nanotechnology* **2016,** *27* (13).
22. Seoudi, R. S.; Dowd, A.; Smith, B. J.; Mechler, A., Structural analysis of bioinspired nano materials with synchrotron far IR spectroscopy. *Phys. Chem. Chem. Phys.* **2016,** *18* (16), 11467-11473.
23. Seoudi, R. S.; Dowd, A.; Del Borgo, M.; Kulkarni, K.; Perlmutter, P.; Aguilar, M. I.; Mechler, A., Amino acid sequence controls the self-assembled superstructure morphology of N-acetylated tri-beta(3)-peptides. *Pure Appl. Chem.* **2015,** *87* (9-10), 1021-1028.
24. Seoudi, R. S.; Del Borgo, M. P.; Kulkarni, K.; Perlmutter, P.; Aguilar, M. I.; Mechler, A., Supramolecular self-assembly of 14-helical nanorods with tunable linear and dendritic hierarchical morphologies. *New J. Chem.* **2015,** *39* (5), 3280-3287.
25. Del Borgo, M. P.; Mechler, A. I.; Traore, D.; Forsyth, C.; Wilce, J. A.; Wilce, M. C. J.; Aguilar, M. I.; Perlmutter, P., Supramolecular Self-Assembly of N-Acetyl-Capped beta-Peptides Leads to Nano- to Macroscale Fiber Formation. *Angew. Chem.-Int. Edit.* **2013,** *52* (32), 8266-8270.
26. Buchanan, C.; Garvey, C. J.; Puskar, L.; Perlmutter, P.; Mechler, A., Coordination crosslinking of helical substituted oligoamide nanorods with Cu(II). *Supramolecular Chemistry* **2020,** *32* (3), 222-232.
27. Buchanan, C.; Garvey, C. J.; Perlmutter, P.; Mechler, A., Co-assembly of helical beta(3)-peptides: a self-assembled analogue of a statistical copolymer. *Pure Appl. Chem.* **2017,** *89* (12), 1809-1816.
28. Craig, C. J.; Goodman, J. L.; Schepartz, A., Enhancing beta(3)-Peptide Bundle Stability by Design. *Chembiochem* **2011,** *12* (7), 1035-1038.
29. Price, J. L.; Horne, W. S.; Gellman, S. H., Structural Consequences of beta-Amino Acid Preorganization in a Self-Assembling alpha/beta-Peptide: Fundamental Studies of Foldameric Helix Bundles. *J. Am. Chem. Soc.* **2010,** *132* (35), 12378-12387.
30. Del Borgo, M. P.; Kulkarni, K.; Tonta, M. A.; Ratcliffe, J. L.; Seoudi, R.; Mechler, A. I.; Perlmutter, P.; Parkington, H. C.; Aguilar, M. I., beta(3)-tripeptides act as sticky ends to self-assemble into a bioscaffold. *APL Bioeng.* **2018,** *2* (2), 9.
31. Mechler, A.; Seoudi, R.; Del Borgo, M. P.; Aguilar, M.-I.; Perlmutter, P., Nano-architecture: creating complex surface structures using supramolecular self-assembly of tripeptides. *Micro/Nano Materials, Devices, and Systems* **2013,** *8923*.
32. Kirby, N. M.; Mudie, S. T.; Hawley, A. M.; Cookson, D. J.; Mertens, H. D. T.; Cowieson, N.; Samardzic-Boban, V., A low-background-intensity focusing small-angle X-ray scattering undulator beamline. *Journal of Applied Crystallography* **2013,** *46*, 1670-1680.
33. Mudie, S. T.; Cookson, D.; Kirby, N.; Hawley, A.; Mertens, H. D. T. In *scatterBrain: An Advanced Software Package for Small Angle Scattering Data Acquisition, Reduction, and Analysis*, 15th International Small-Angle Scattering Conference, Sydney, McGillivray, D. J.; Trewhella, J.; Gilbert, E. P.; Hanley, T. L., Eds. Australian Nuclear Science and Technology Organisation: Sydney, 2012.
34. Doucet, M.; Cho, J.; Alina, G.; Bakker, J.; Bouwman, W.; Butler, P.; Campbell, K.; Gonzales, M.; Heenan, R.; Jackson, A.; Juhas, P.; King, S.; Kienzle, P.; Krzywon, J.; Markvardsen, A.; Nielsen, T.; O'Driscoll, L.; Potrzebowski, W.; R., F. L.; Richter, T.; Rozycko, P.; Washington, A. *SASView V4.1*, 2017.
35. Feigin, L. A.; Svergun, D. I., *Structure Analysis by Small-Angle X-ray and Neutron scattering*. Plenum: New York, 1987.
36. Onsager, L., THE EFFECTS OF SHAPE ON THE INTERACTION OF COLLOIDAL PARTICLES. *Annals of the New York Academy of Sciences* **1949,** *51* (4), 627-659.
37. Pedersen, J. S., Analysis of small-angle scattering data from colloids and polymer solutions: modeling and least-squares fitting. *Advances in Colloid and Interface Science* **1997,** *70*, 171-210.
38. Ilavsky, J.; Jemian, P. R., Irena: tool suite for modeling and analysis of small-angle scattering. *Journal of Applied Crystallography* **2009,** *42*, 347-353.
39. Svergun, D.; Barberato, C.; Koch, M. H. J., CRYSOL - A program to evaluate x-ray solution scattering of biological macromolecules from atomic coordinates. *J. Appl. Crystallogr.* **1995,** *28*, 768-773.
40. Bandekar, J., AMIDE MODES AND PROTEIN CONFORMATION. *Biochimica Et Biophysica Acta* **1992,** *1120* (2), 123-143.
41. Matei, A.; Drichko, N.; Gompf, B.; Dressel, M., Far-infrared spectra of amino acids. *Chemical Physics* **2005,** *316* (1-3), 61-71.
42. Wolpert, M.; Hellwig, P., Infrared spectra and molar absorption coefficients of the 20 alpha amino acids in aqueous solutions in the spectral range from 1800 to 500 cm(-1). *Spectrochim. Acta A* **2006,** *64* (4), 987-1001.
43. Barth, A., The infrared absorption of amino acid side chains. *Prog. Biophys. Mol. Bio.* **2000,** *74* (3-5), 141-173.
44. Kong, J.; Yu, S., Fourier transform infrared spectroscopic analysis of protein secondary structures. *Acta Biochim Biophys Sin* **2007,** *39* (8), 549-559.
45. Barth, A., Infrared spectroscopy of proteins. *Biochim. Biophys. Acta, Bioenerg.* **2007,** *1767* (9), 1073-1101.
46. Jansen, T. L.; Dijkstra, A. G.; Watson, T. M.; Hirst, J. D.; Knoester, J., Modeling the amide I bands of small peptides. *J. Chem. Phys.* **2006,** *125* (4), 9.
47. Barth, A.; Zscherp, C., What vibrations tell us about proteins. *Q. Rev. Biophys.* **2002,** *35* (4), 369-430.
48. Vasantha, B.; Yamanappa, H.; Raghothama, S.; Balaram, P., Conformational properties and aggregation of homo-oligomeric beta(3)(R)-valine peptides in organic solvents. *Biopolymers* **2017,** *108* (3).
49. Dutot, L.; Gaucher, A.; Elkassimi, K.; Drapeau, J.; Wakselman, M.; Mazaleyrat, J.-P.; Peggion, C.; Formaggio, F.; Toniolo, C., Synthesis and characterisation of helical beta-peptide architectures that contain (S)-beta(3)-HDOPA (crown ether) derivatives. *Chem.: Eur. J* **2008,** *14* (10), 3154-3163.

50. Horne, W. S.; Gellman, S. H., Foldamers with Heterogeneous Backbones. *Accounts Chem. Res.* **2008,** *41* (10), 1399-1408.
51. Arvidsson, P. I.; Rueping, M.; Seebach, D., Design, machine synthesis, and NMR-solution structure of a beta-heptapeptide forming a salt-bridge stabilised 3(14)-helix in methanol and in water. *Chem. Commun.* **2001,** (7), 649-650.
52. Seebach, D.; Matthews, J. L., beta-peptides: a surprise at every turn. *Chem. Commun.* **1997,** (21), 2015-2022.